

# Dalton Transactions

Accepted Manuscript



This is an *Accepted Manuscript*, which has been through the Royal Society of Chemistry peer review process and has been accepted for publication.

*Accepted Manuscripts* are published online shortly after acceptance, before technical editing, formatting and proof reading. Using this free service, authors can make their results available to the community, in citable form, before we publish the edited article. We will replace this *Accepted Manuscript* with the edited and formatted *Advance Article* as soon as it is available.

You can find more information about *Accepted Manuscripts* in the [Information for Authors](#).

Please note that technical editing may introduce minor changes to the text and/or graphics, which may alter content. The journal's standard [Terms & Conditions](#) and the [Ethical guidelines](#) still apply. In no event shall the Royal Society of Chemistry be held responsible for any errors or omissions in this *Accepted Manuscript* or any consequences arising from the use of any information it contains.

Manuscript for *Dalton Trans.*

# First example of Tb<sub>3</sub>-containing metallopolymer-type hybrid materials with efficient and high color-purity green luminescence

Zhao Zhang,<sup>a</sup> Heini Feng,<sup>a</sup> Lin Liu,<sup>a</sup> Chao Yu,<sup>a</sup> Xingqiang Lü,<sup>\*a</sup> Xunjin Zhu,<sup>b</sup>  
Wai-Kwok Wong,<sup>b</sup> Richard A. Jones,<sup>c</sup> Mei Pan<sup>d</sup> and Chengyong Su<sup>\*d</sup>

<sup>a</sup>*School of Chemical Engineering, Shaanxi Key Laboratory of Degradable Medical Material, Northwest University, Xi'an 710069, Shaanxi, P. R. China*

<sup>b</sup>*Department of Chemistry, Hong Kong Baptist University, Waterloo Road, Kowloon Tong, Hong Kong, P. R. China*

<sup>c</sup>*Department of Chemistry and Biochemistry, The University of Texas at Austin, 1 University Station A5300, Austin, TX 78712-0165, United States*

<sup>d</sup>*MOE Laboratory of Bioinorganic and Synthetic Chemistry/KLGH EI of Environment and Energy Chemistry, School of Chemistry and Chemical Engineering, Sun Yat-Sen University, Guangzhou 510275, Guangdong, China*

To whom correspondence should be addressed.

\*Xingqiang Lü: 86-29-88302312(o); E-mail: [lvxq@nwu.edu.cn](mailto:lvxq@nwu.edu.cn)

\*Chengyong Su: 86-20-84115178(o); E-mail: [cesscy@mail.sysu.edu.cn](mailto:cesscy@mail.sysu.edu.cn)

## Abstract

In the series of homo-leptic trinuclear complexes  $\{[\text{Ln}_3(\text{L})_4\text{Cl}_4(\text{MeOH})(\text{H}_2\text{O})]\cdot\text{Cl}\}$  ( $\text{Ln} = \text{La}$ , **1**;  $\text{Ln} = \text{Eu}$ , **2**;  $\text{Ln} = \text{Tb}$ , **3** or  $\text{Ln} = \text{Gd}$ , **4**) self-assembled from the allyl-modified benzimidazole-type ligand **HL** (4-allyl-2-(1*H*-benzo[d]imidazol-2-yl)-6-methoxyphenol) and  $\text{LnCl}_3\cdot 6\text{H}_2\text{O}$ , the suitable energy level match endows the efficient green luminescence ( $\Phi_{\text{overall}} = 72\%$ ) of the  $\text{Tb}_3$ -arrayed complex **3**. The copolymerization between each of these complex monomers **1-4** with C=C-containing MMA (methyl methacrylate) or NBE (norbornene) shows that the degradative chain transfer of the terminal four flexible ally groups within restrains their radical polymerization with MMA while does not hinder their effective ring-opening metathesis polymerization (ROMP) with NBE. Thus, two kinds of PMMA-supported doping hybrid materials **1@PMMA**, **2@PMMA**, **3@PMMA** and **4@PMMA** and PNBE-supported metallopolymer-type hybrid materials **Poly(NBE-1)**, **Poly(NBE-2)**, **Poly(NBE-3)** and **Poly(NBE-4)** are obtained, respectively. Especially for both **3@PMMA** and **Poly(NBE-3)** with high color-purity characteristic green emission of  $\text{Tb}^{3+}$  ion, the improved physical properties including the significantly enhanced luminescence ( $\Phi_{\text{overall}} = 76\%$  or  $83\%$ ) are observed, and the covalently-bonding endows the higher-concentration self-quenching as compared to the physical doping.

**Keyword:** PMMA-supported doping or PNBE-supported metallopolymer-type hybrid material;  $\text{Tb}_3$ -arrayed benzimidazole-type complex; Radical polymerization or ROMP; Energy transfer

## 1. Introduction

Due to the large Stokes shift, ms-grade long lifetime and characteristic narrow line-like emission of  $\text{Eu}^{3+}$  or  $\text{Tb}^{3+}$  ion, there has been a growing interest on the development of new kinds of high color-purity  $\text{Eu}^{3+}$ - (red) or  $\text{Tb}^{3+}$ -based (green) optical materials with potential applications in organic light-emitting diodes (OLEDs),<sup>1</sup> white light-emitting devices,<sup>2</sup> color-tuning pigments<sup>3</sup> or biological fluoro-immunoassay.<sup>4</sup> However, limited by the forbidden parity from f-f transitions of these two inorganic  $\text{Ln}^{3+}$  ions, the molar absorption coefficients are normally very low ( $\epsilon = 0.01\text{-}10 \text{ M}^{-1}\text{cm}^{-1}$ ). From the viewpoint of effective sensitization, suitable chromophore is required to allow for indirect population of those  $\text{Ln}^{3+}$  ions' emissive excited states through ligand excitation ("antenna effect").<sup>5</sup> For this purpose, the compatibility between the excited state level of the chromophore and the accepting level of the corresponding  $\text{Ln}^{3+}$  ion should be realized<sup>6</sup> in these luminescent  $\text{Ln}^{3+}$ -complexes besides the avoidance of the non-radiative deactivation by OH-, NH- or CH-oscillators around the  $\text{Ln}^{3+}$  ion.<sup>7</sup> Nevertheless, the  $\text{Ln}^{3+}$ -complexes generally present low thermal stability and poor mechanical property, giving rise to another parallel challenge.

In order to overcome these deficiencies and simultaneously improve the photo-physical property of these  $\text{Ln}^{3+}$ -complexes, one of simple while effective solutions is through physical doping into a host inorganic or organic polymeric matrix.<sup>8</sup> On the other hand, an alternative approach is to trapping the  $\text{Ln}^{3+}$ -complex into a silica-based host<sup>9</sup> or a polymer backbone<sup>10</sup> with covalent bonds for the formation of grafting-type inorganic-organic hybrid materials. By contrast,  $\text{Ln}^{3+}$ -containing metallopolymer,<sup>11</sup> as a unique class of grafted hybrid materials, possess both the beneficial property of the inorganic  $\text{Ln}^{3+}$  ions and the attractive features

including mechanical strength, flexibility, ease of processing and low cost of organic polymers. This advantage, especially compared with  $\text{Ln}^{3+}$ -containing doping hybrid materials, endows the ability to effectively resolve the high homogeneity and clustering of emitters and makes them more ideal as optoelectronic materials. Till now, to the best of our knowledge, the developed  $\text{Ln}^{3+}$ -containing metallopolymer are usually limited from the mononuclear  $\text{Ln}^{3+}$ -complexes through coupling,<sup>12</sup> ring-opening polymerization,<sup>13</sup> radical polymerization<sup>14</sup> or electro-polymerization,<sup>15</sup> and few systems fabricated from d-f heterometallic<sup>16</sup> or f-f poly-metallic complexes.<sup>17</sup> In our recent reports, through the radical copolymerization of the divinyl-modified  $\text{ZnLn}$  or  $\text{Zn}_2\text{Ln}$  ( $\text{Ln} = \text{Nd}$ ,  $\text{Yb}$  or  $\text{Er}$ ) Salen-type Schiff-base complex monomer and another  $\text{C}=\text{C}$ -containing monomer, two examples of near-infrared (NIR) luminescent  $\text{ZnLn}$ <sup>16b, 16c</sup> or  $\text{Zn}_2\text{Ln}$ -containing<sup>16d</sup> metallopolymer are constructed. Moreover, another example of NIR luminescent metallopolymer based on allyl-modified  $\text{Ln}_4(\text{Salen})_4$  ( $\text{Ln} = \text{Nd}$  or  $\text{Yb}$ ) complexes is successfully built by the controlled ring-opening metathesis polymerization (ROMP) with norbornene (NBE).<sup>17</sup> In the two kinds of metallopolymer, the additive electronic communication between the homo- or hetero-multiple metal centers actually induces more efficient energy transfer. In consideration of the relatively higher first excited state ( $17286\text{ cm}^{-1}$ ,  $^5\text{D}_0$  for  $\text{Eu}^{3+}$ ;  $20545\text{ cm}^{-1}$ ,  $^5\text{D}_4$  for  $\text{Tb}^{3+}$ ) of visible luminescent  $\text{Eu}^{3+}$  or  $\text{Tb}^{3+}$  ion than that ( $11257\text{ cm}^{-1}$ ,  $^4\text{F}_{3/2}$  for  $\text{Nd}^{3+}$ ;  $10400\text{ cm}^{-1}$ ,  $^2\text{F}_{5/2}$  for  $\text{Yb}^{3+}$ ,  $6610\text{ cm}^{-1}$ ,  $^4\text{I}_{13/2}$  for  $\text{Er}^{3+}$ ) of NIR luminescent  $\text{Nd}^{3+}$ ,  $\text{Yb}^{3+}$  or  $\text{Er}^{3+}$  ion,<sup>18</sup> new organic ligands also with unsaturated  $\text{C}=\text{C}$  functions while not vinyl- or allyl-modified Salen-type Schiff-base ligands need to be designed, where the polymerizable multi-metallic  $\text{Eu}^{3+}$  or  $\text{Tb}^{3+}$  complex monomer with higher  $^3\pi-\pi^*$  energy level matched well with the first excited state of  $\text{Eu}^{3+}$  or  $\text{Tb}^{3+}$  ion

can also be copolymerized with other C=C-containing monomers. Thus, new polymetallic-containing metallopolymers with  $\text{Eu}^{3+}$ - or  $\text{Tb}^{3+}$ -based high color-purity visible emission are expected. Herein, through the self-assembly of the allyl-modified benzimidazole-type ligand **HL** and  $\text{LnCl}_3 \cdot 6\text{H}_2\text{O}$  ( $\text{Ln} = \text{La}, \text{Eu}, \text{Tb}$  or  $\text{Gd}$ ), a series of homo-leptic trinuclear complexes  $\{[\text{Ln}_3(\text{L})_4\text{Cl}_4(\text{MeOH})(\text{H}_2\text{O})] \cdot \text{Cl}\}$  ( $\text{Ln} = \text{La}$ , **1**;  $\text{Ln} = \text{Eu}$ , **2**;  $\text{Ln} = \text{Tb}$ , **3** or  $\text{Ln} = \text{Gd}$ , **4**) are obtained, respectively. The series of  $\text{Ln}_3$ -arrayed ( $\text{Ln} = \text{Eu}$  or  $\text{Tb}$ ) complex monomers with four terminal allyl groups should be copolymerized with MMA or NBE, and thus, the first example of high color-purity  $\text{Eu}^{3+}$ - or  $\text{Tb}^{3+}$ -based trimetallic emissive metallopolymers could be anticipated.

## 2. Experimental

### Materials and methods

High performance liquid chromatography (HPLC) grade tetrahydrofuran (THF) was purchased from Fisher Scientific and purified over solvent columns. Other solvents were used as received from Sigma Aldrich and stored over 3 Å activated molecule sieves. Methyl methacrylate (MMA) was dried over  $\text{CaH}_2$ , distilled and stored under dried  $\text{N}_2$  prior to use. Azobis(isobutyronitrile) (AIBN) was purified by recrystallization twice from absolute MeOH prior to use. Other chemicals containing Hoveyda-Grubbs II (H-Grubbs II) and norborene (NBE) were commercial products of reagent grade and were used without further purification. All manipulations of air and water sensitive compounds were carried out under dried  $\text{N}_2$  using the standard Schlenk line techniques. Elemental analyses were performed on a Perkin-Elmer 240C elemental analyzer. Infrared spectra were recorded on a Nicolet Nagna-IR 550

spectrophotometer in the region 4000-400  $\text{cm}^{-1}$  using KBr pellets.  $^1\text{H}$  NMR spectra were recorded on a JEOL EX 400 spectrometer with  $\text{SiMe}_4$  as internal standard in  $\text{CD}_3\text{CN}$ ,  $\text{CDCl}_3$  and/or  $\text{DMSO}-d_6$  at room temperature. ESI-MS was performed on a Finnigan  $\text{LCQ}^{\text{DECA}}$  XP HPLC- $\text{MS}_n$  mass spectrometer with a mass to charge ( $m/z$ ) range of 4000 using a standard electrospray ion source and MeCN as solvent. Electronic absorption spectra in the UV/Visible region and diffuse reflection (DR) spectra were recorded with a Cary 300 UV spectrophotometer, steady-state visible fluorescence and PL excitation spectra were recorded on a Photon Technology International (PTI) Alpha scan spectrofluorometer, and visible decay spectra were recorded on a pico- $\text{N}_2$  laser system (PTI Time Master). The quantum yield ( $\Phi_{\text{overall}}$ ) of visible luminescence for each sample in solution was determined by the relative comparison procedure, using a reference of a known quantum yield (quinine sulfate in dilute  $\text{H}_2\text{SO}_4$  solution,  $\Phi_r = 0.546$ ). The quantum yield ( $\Phi_{\text{overall}}$ ) of visible luminescence for each solid state sample was determined by absolute method using an integrating sphere<sup>19</sup> (150 nm diameter,  $\text{BaSO}_4$  coating) on Edinburgh Instrument FLS928. Three parallel measurements were carried out for each sample, so that the presented  $\Phi_{\text{overall}}$  value corresponds to the arithmetic mean value with the estimated errors of 10%. Gel permeation chromatography (GPC) analyses of the polymers were performed using a Waters 1525 binary pump coupled to a Waters 2414 refractive index detector with HPLC THF as the eluant on American Polymer Standard 10  $\mu\text{m}$  particle size, linear mixed bed packing columns. The GPC was calibrated using polystyrene standards. The powder X-ray diffraction (PXRD) patterns were recorded on a D/Max-III A diffractometer with graphite-monochromatized  $\text{Cu K}\alpha$  radiation ( $\lambda = 1.5418 \text{ \AA}$ ). Thermogravimetric (TG) analyses were carried out on a NETZSCH TG 209 instrument under

flowing nitrogen by heating the samples from 25 to 600 °C.

### Synthesis of 5-allyl-2-hydroxy-3-methoxy-benzaldehyde

5-Allyl-2-hydroxy-3-methoxy-benzaldehyde was obtained by the Williamson synthesis from *o*-vanillin (6.08 g, 40 mmol) and allyl bromide (12.0 mL, 140 mmol) as the starting materials in the presence of anhydrous K<sub>2</sub>CO<sub>3</sub> (11.06 g, 80 mmol) and the subsequent *para* Claisen rearrangement according to a well-established procedure from the literature.<sup>17</sup> Yield: 3.92 g, 51%. Element analysis (%): calcd for C<sub>11</sub>H<sub>12</sub>O<sub>3</sub> (192.21): C, 68.74; H, 6.29. Found: C, 68.72; H, 6.34. <sup>1</sup>H NMR (400 MHz, CDCl<sub>3</sub>): δ (ppm) 11.10 (s, 1H, -OH), 9.90 (s, 1H, -CHO), 6.99 (s, 1H, -Ph), 6.95 (s, 1H, -Ph), 5.97 (m, 1H, -CH=C), 5.13 (m, 2H, =CH<sub>2</sub>), 3.91 (s, 3H, -OMe), 3.38 (s, 2H, -CH<sub>2</sub>).

### Synthesis of diallyl-modified Salen-type Schiff-base precursor H<sub>2</sub>L<sup>0</sup> (H<sub>2</sub>L<sup>0</sup> = N,N'-bis(5-allyl-3-methoxy-salicylidene)phenylene-1,2-diamine)

To a stirred solution *o*-phenylenediamine (0.55 g, 5 mmol) in absolute EtOH (20 mL), 5-allyl-2-hydroxy-3-methoxy-benzaldehyde (1.92 g, 10 mmol) was added, and the resultant mixture was continuously stirred under N<sub>2</sub> atmosphere at room temperature for 12 h. The insoluble red precipitate was filtered and washed with cold diethyl ether to give a red polycrystalline solid. Yield: 1.46 g, 64%. Element analysis (%): calcd for C<sub>28</sub>H<sub>28</sub>N<sub>2</sub>O<sub>4</sub> (456.64): C, 73.66; H, 6.18; N 6.14. Found: C, 73.75; H, 6.15; N, 6.06. FT-IR (KBr, cm<sup>-1</sup>): 3320 (b), 3070 (w), 2993 (w), 2943 (w), 2898 (w), 2839 (w), 1620 (s), 1581 (m), 1475 (s), 1394 (m), 1344 (w), 1267 (vs), 1230 (w), 1209 (w), 1161 (m), 993 (s), 966 (w), 908 (m), 840



(w), 800 (w), 746 (w), 686 (w), 600 (w), 545 (w), 503 (w), 480 (w).  $^1\text{H}$  NMR (400 MHz,  $\text{CD}_3\text{CN}$ ):  $\delta$  (ppm) 13.16 (s, 2H, -OH), 8.71 (s, 2H, -CH=N), 7.37 (m, 4H, -Ph), 6.94 (s, 4H, -Ph), 6.01 (m, 2H, -CH=C), 5.10 (m, 4H, =CH<sub>2</sub>), 3.86 (s, 6H, -OMe), 3.36 (m, 4H, -CH<sub>2</sub>).

**Synthesis of allyl-modified benzimidazole-type ligand HL (HL = 4-allyl-2-(1*H*-benzo[d]imidazol-2-yl)-6-methoxyphenol)**

The solution of the diallyl-modified Salen-type Schiff-base precursor **H<sub>2</sub>L<sup>0</sup>** (4.56 g, 10 mmol) in absolute MeOH (20 mL) was refluxed under N<sub>2</sub> atmosphere for 36 h, where the color of the solution changed from dark red to brown and white. After cooling to room temperature, the volatile materials were removed under vacuum, and the colorless solid residue (**HL**) remained was washed with absolute EtOH and dried under vacuum. Yield: 1.96 g, 70%. Element analysis (%): calcd for C<sub>17</sub>H<sub>16</sub>N<sub>2</sub>O<sub>2</sub> (280.33): C, 72.84; H, 5.75; N, 9.99. Found: C, 72.76; H, 5.87; N, 9.91. FT-IR (KBr, cm<sup>-1</sup>): 3651 (w), 3524 (w), 3464 (w), 3067 (w), 2970 (w), 2928 (w), 2907 (w), 2837 (w), 2766 (w), 2731 (w), 2654 (w), 2596 (w), 2531 (w), 2486 (w), 2293 (w), 2259 (w), 2212 (w), 2116 (w), 2021 (w), 1977 (w), 1933 (w), 1894 (w), 1846 (w), 1827 (w), 1776 (w), 1722 (w), 1624 (s), 1599 (m), 1499 (s), 1454 (s), 1398 (s), 1342 (w), 1254 (vs), 1146 (s), 1063 (s), 997 (s), 964 (w), 914 (m), 851 (m), 800 (m), 748 (m), 681 (w), 615 (m), 548 (w), 494 (w), 434 (w).  $^1\text{H}$  NMR (400 MHz,  $\text{CD}_3\text{CN}$ ):  $\delta$  (ppm) 12.99 (s, 1H, -NH), 11.09 (s, 1H, -OH), 7.72 (d, 1H, -Ph), 7.60 (d, 1H, -Ph), 7.31 (m, 3H, -Ph), 6.94 (s, 1H, -Ph), 6.09 (m, 1H, -CH=C), 5.17 (m, 2H, =CH<sub>2</sub>), 3.90 (s, 3H, -OMe), 3.44 (d, 2H, -CH<sub>2</sub>).

**Synthesis of homo-leptic trinuclear complexes {[Ln<sub>3</sub>(L)<sub>4</sub>Cl<sub>4</sub>(MeOH)(H<sub>2</sub>O)]·Cl} (Ln = La,**

**1; Ln = Eu, 2; Ln = Tb, 3 or Ln = Gd, 4)**

The CH<sub>2</sub>Cl<sub>2</sub>-MeOH solution (10 mL, V/V = 1/1) containing **HL** (168 mg, 0.6 mmol) and Et<sub>3</sub>N (84 μL, 0.6 mmol) was stirred for 30 min at RT, then a solution of LnCl<sub>3</sub>·6H<sub>2</sub>O (0.6 mmol, Ln = La, 212 mg; Ln = Eu, 220 mg; Ln = Tb, 224 mg or Ln = Gd, 223 mg) in absolute MeOH (5 mL) was added and the mixture was refluxed under N<sub>2</sub> atmosphere for 3 h, respectively. After cooling to RT, the resultant respective clear yellow solution was filtered, and diethyl ether was allowed to diffuse slowly into the filtrate at RT. Pale yellow microcrystalline products were obtained in about two weeks, respectively.

For **1**: Yield: 193 mg, 73%. Element analysis (%): calcd for C<sub>69</sub>H<sub>66</sub>N<sub>8</sub>O<sub>10</sub>Cl<sub>5</sub>La<sub>3</sub> (1761.31): C, 47.05; H, 3.78; N, 6.36. Found: C, 47.15; H, 3.94; N, 6.28. FT-IR (KBr, cm<sup>-1</sup>): 3380 (b), 3220 (s), 2977 (s), 2940 (s), 2740 (m), 2679 (s), 2491 (w), 1620 (s), 1570 (s), 1507 (vs), 1465 (s), 1430 (s), 1399 (m), 1351 (m), 1276 (m), 1246 (s), 1211 (m), 1171 (w), 1133 (m), 1057 (s), 1039 (w), 1010 (w), 994 (s), 917 (w), 851 (m), 820 (w), 770 (s), 748 (s), 683 (w), 654 (w), 623 (w), 585 (w), 569 (w), 530 (w), 498 (w). <sup>1</sup>H NMR (400 MHz, DMSO-*d*<sub>6</sub>): δ (ppm) 13.17 (s, 4H, -NH), 8.24 (m, 1H, -OH), 7.79 (m, 2H, -Ph), 7.71 (m, 4H, -Ph), 7.61 (m, 2H, -Ph), 7.49 (m, 4H, -Ph), 7.39 (m, 3H, -Ph), 7.27 (m, 3H, -Ph), 7.18 (m, 6H, -Ph), 6.03 (m, 4H, -CH=C), 5.13 (m, 8H, =CH<sub>2</sub>), 3.87 (s, 3H, MeOH), 3.83 (s, 12H, -OMe), 3.33 (s, 8H, -CH<sub>2</sub>). ESI-MS (in MeCN) *m/z*: 1725.86 (100%), [M-Cl]<sup>+</sup>; 1762.32 (18%), [M+H]<sup>+</sup>.

For **2**: Yield: 192 mg, 71%. Element analysis (%): calcd for C<sub>69</sub>H<sub>66</sub>N<sub>8</sub>O<sub>10</sub>Cl<sub>5</sub>Eu<sub>3</sub> (1800.48): C, 46.03; H, 3.69; N, 6.22. Found: C, 46.06; H, 3.82; N, 6.15. FT-IR (KBr, cm<sup>-1</sup>): 3373 (b), 3210 (m), 2945 (m), 2841 (m), 1622 (s), 1571 (s), 1522 (m), 1487 (vs), 1463 (s), 1445 (s), 1424 (s), 1345 (m), 1307 (w), 1280 (m), 1243 (s), 1202 (m), 1140 (m), 1057 (s), 1012 (w),

1000 (s), 957 (w), 910 (m), 865 (w), 850 (w), 817 (m), 766 (s), 748 (s), 686 (w), 654 (w), 624 (w), 574 (w), 499 (w). ESI-MS (in MeCN)  $m/z$ : 1765.02 (100%),  $[M-Cl]^+$ ; 1801.48 (16%),  $[M+H]^+$ .

For **3**: Yield: 189 mg, 69%. Element analysis (%): calcd for  $C_{69}H_{66}N_8O_{10}Cl_5Tb_3$  (1821.37): C, 45.50; H, 3.65; N, 6.15. Found: C, 45.47; H, 3.74; N, 6.10. FT-IR (KBr,  $cm^{-1}$ ): 3390 (b), 3227 (m), 2975 (m), 2941 (m), 2737 (m), 2677 (m), 2490 (w), 1621 (s), 1570 (s), 1507 (s), 1495 (vs), 1464 (s), 1431 (m), 1398 (m), 1350 (w), 1278 (w), 1245 (s), 1211 (w), 1171 (w), 1133 (w), 1057 (m), 1037 (w), 995 (s), 917 (w), 825 (w), 821 (w), 770 (s), 747 (m), 688 (w), 655 (w), 623 (w), 589 (w), 502 (w). ESI-MS (in MeCN)  $m/z$ : 1785.92 (100%),  $[M-Cl]^+$ ; 1822.38 (13%),  $[M+H]^+$ .

For **4**: Yield: 185 mg, 68%. Element analysis (%): calcd for  $C_{69}H_{66}N_8O_{10}Cl_5Gd_3$  (1816.35): C, 45.63; H, 3.66; N, 6.17. Found: C, 45.97; H, 3.81; N, 6.08. FT-IR (KBr,  $cm^{-1}$ ): 3378 (b), 3219 (m), 2977 (m), 2941 (m), 2739 (m), 2679 (m), 2492 (w), 1620 (s), 1571 (s), 1507 (s), 1465 (vs), 1434 (s), 1399 (m), 1352 (m), 1278 (m), 1246 (s), 1211 (m), 1170 (w), 1133 (m), 1057 (s), 1037 (w), 1010 (w), 995 (s), 917 (w), 852 (m), 820 (w), 771 (s), 748 (s), 687 (w), 654 (w), 623 (w), 589 (w), 569 (w), 531 (w), 499 (w). ESI-MS (in MeCN)  $m/z$ : 1780.89 (100%),  $[M-Cl]^+$ ; 1817.35 (14%),  $[M+H]^+$ .

### Determination of the crystal structure

Single crystals for  $3 \cdot 2MeOH \cdot 4H_2O$  of suitable dimensions were mounted onto thin glass fibers. All the intensity datas were collected on a Bruker SMART CCD diffractometer (Mo-K $\alpha$  radiation and  $\lambda = 0.71073 \text{ \AA}$ ) in  $\Phi$  and  $\omega$  scan modes. Structures were solved by

Direct methods followed by difference Fourier syntheses, and then refined by full-matrix least-squares techniques against  $F^2$  using SHELXTL.<sup>20</sup> All other non-hydrogen atoms were refined with anisotropic thermal parameters. Absorption corrections were applied using SADABS.<sup>21</sup> All hydrogen atoms were placed in calculated positions and refined isotropically using a riding model. Crystallographic data and refinement parameters for the complexes are presented in Table 1. Relevant atomic distances and bond angles are collected in Table 1S. CCDC reference number 1035177 is for **3**·2MeOH·4H<sub>2</sub>O.

### Synthesis of PMMA-supported doping hybrid materials **1@PMMA**, **2@PMMA**, **3@PMMA** and **4@PMMA**

The homogeneous polymerization of MMA and each of complexes  $\{[Ln_3(L)_4Cl_4(MeOH)(H_2O)] \cdot Cl\}$  ( $Ln = La$ , **1**;  $Ln = Eu$ , **2**;  $Ln = Tb$ , **3** or  $Ln = Gd$ , **4**) with a stipulated feeding molar ratio (200:1, 400:1, 600:1 or 800:1) in activation with AIBN was carried out in a Fisher-Porter glass reactor and protected by dried N<sub>2</sub> according to the typical procedure.<sup>22</sup> A mixture of MMA (2.7 mL, 25.3 mmol) in activation with AIBN (37.6 mg, 1.5 mol % of MMA) and  $\{[Ln_3(L)_4Cl_4(MeOH)(H_2O)] \cdot Cl\}$  (0.063 mmol;  $Ln = La$  (**1**), 111 mg;  $Ln = Eu$  (**2**), 114 mg;  $Ln = Tb$  (**3**), 115 mg or  $Ln = Gd$  (**4**), 116 mg) was dissolved in dry xylene (30 mL), and the resultant homogeneous solution was purged with N<sub>2</sub> for 10 min and sealed under a reduced N<sub>2</sub> atmosphere. The solution was heated to 60 °C with continuous stirring for 24 h. The viscous mixture was diluted with dry THF (20 mL) and precipitated with absolute diethyl ether (50 mL) for three times. The resulting solid products were collected by filtration and dried at 45 °C under vacuum to constant weight, respectively.

For **1@PMMA** (400:1): Yield: 91%. FT-IR (KBr,  $\text{cm}^{-1}$ ): 3631 (w), 3381 (m), 3221 (w), 3300 (w), 2996 (m), 2949 (m), 2844 (w), 1732 (vs), 1625 (m), 1570 (w), 1505 (w), 1460 (m), 1390 (s), 1348 (w), 1309 (w), 1255 (w), 1201 (w), 1058 (w), 1045 (w), 1018 (w), 1002 (w), 960 (w), 867 (w), 823 (w), 767 (m), 746 (m), 684 (w), 658 (w), 585 (w), 555 (w), 514 (w), 466 (w).  $^1\text{H}$  NMR (400 MHz,  $\text{DMSO}-d_6$ - $\text{CDCl}_3$ , v/v = 10:1):  $\delta$  (ppm) 13.12 (s, 4H, -NH), 8.20 (m, 1H, -OH), 7.78 (m, 2H, -Ph), 7.70 (m, 4H, -Ph), 7.61 (m, 2H, -Ph), 7.48 (m, 4H, -Ph), 7.38 (m, 3H, -Ph), 7.27 (m, 3H, -Ph), 7.17 (m, 6H, -Ph), 6.01 (m, 4H, -CH=C), 5.11 (m, 8H, =CH<sub>2</sub>), 3.86 (s, 3H, MeOH), 3.83 (s, 12H, -OMe), 3.56 (s, 330H, -COOMe), 3.32 (s, 8H, -CH<sub>2</sub>), 1.85 (b, 220H, -CH<sub>2</sub>), 0.91 (m, 330H, -CH<sub>3</sub>).

For **2@PMMA** (400:1): Yield: 90%. FT-IR (KBr,  $\text{cm}^{-1}$ ): 3624 (w), 3383 (m), 3219 (w), 3301 (w), 3070 (w), 2996 (m), 2950 (m), 2841 (w), 1731 (vs), 1624 (m), 1570 (w), 1501 (w), 1466 (w), 1391 (s), 1345 (w), 1308 (w), 1252 (w), 1200 (w), 1059 (w), 1041 (w), 1017 (w), 1000 (w), 966 (w), 868 (w), 820 (w), 765 (m), 746 (m), 681 (w), 650 (w), 580 (w), 551 (w), 510 (w), 461 (w).

For **3@PMMA** (200:1, 400:1, 600:1 and 800:1): Yield: 83% (200:1); 89% (400:1); 91% (600:1); 92% (800:1). FT-IR (KBr,  $\text{cm}^{-1}$ ): 3620 (w), 3379 (m), 3222 (w), 3301 (w), 2998 (m), 2948 (m), 2841 (w), 1731 (vs), 1621 (m), 1570 (w), 1507 (w), 1460 (m), 1391 (s), 1345 (w), 1309 (w), 1256 (w), 1201 (w), 1056 (w), 1048 (w), 1017 (w), 1002 (w), 962 (w), 867 (w), 823 (w), 764 (m), 746 (m), 686 (w), 658 (w), 581 (w), 551 (w), 514 (w), 462 (w).

For **4@PMMA** (400:1): Yield: 88%. FT-IR (KBr,  $\text{cm}^{-1}$ ): 3627 (w), 3380 (m), 3220 (w), 3305 (w), 3070 (w), 2997 (m), 2949 (m), 2842 (w), 1732 (vs), 1625 (m), 1571 (w), 1505 (w), 1460 (w), 1392 (s), 1347 (w), 1309 (w), 1254 (w), 1201 (w), 1057 (w), 1046 (w), 1018 (w),

1002 (w), 961 (w), 867 (w), 822 (w), 767 (m), 743 (m), 684 (w), 652 (w), 585 (w), 554 (w), 512 (w), 465 (w).

**Synthesis of PNBE-supported metallopolymer-type hybrid materials Poly(NBE-1), Poly(NBE-2), Poly(NBE-3) and Poly(NBE-4)**

The homogeneous copolymerization of NBE and each of complexes **1-4** with a stipulated feeding molar ratio (200:1, 400:1, 600:1 or 800:1) in activation with H-Grubbs II was carried out in a Fisher-Porter glass reactor and protected by dried N<sub>2</sub>. To a solution of the complex  $\{[Ln_3(L)_4Cl_4(MeOH)(H_2O)] \cdot Cl\}$  (0.02 mmol, Ln = La (**1**), 35.4 mg; Ln = Eu (**2**), 35.8 mg; Ln = Tb (**3**), 36.2 mg or Ln = Gd (**4**), 36.4 mg) in dry CHCl<sub>3</sub> (30 mL), NBE (8 mmol, 752 mg) and H-Grubbs II (1.5 mol-% of NBE; 11.3 mg, added in three times: 7 mg, 2.3 mg and 2 mg, respectively) were added, and the resultant homogeneous solution was purged with N<sub>2</sub> for 10 min and sealed under a reduced N<sub>2</sub> atmosphere. The mixture was stirred at RT for 72 h. Subsequently, ethyl vinyl ether (1 mL) was added to quench the reaction. Each of the obtained products was precipitated as viscous substance by slow dropping into cold EtOH. The resulting solids were collected by filtration and dried at 45 °C under vacuum to constant weight, respectively.

For **Poly(NBE-1)** (400:1): Yield: 79%. FT-IR (KBr, cm<sup>-1</sup>): 3313 (b), 2943 (m), 2862 (s), 2733 (w), 2603 (m), 2530 (w), 2495 (w), 1994 (w), 1772 (m), 1710 (m), 1662 (w), 1616 (w), 1490 (s), 1448 (s), 1348 (w), 1257 (s), 1205 (m), 1145 (w), 1037 (s), 966 (vs), 912 (w), 864 (w), 821 (s), 744 (w), 698 (vs), 671 (w), 580 (w), 497 (w), 439 (w). <sup>1</sup>H NMR (400 MHz, DMSO-*d*<sub>6</sub>-CDCl<sub>3</sub>, v/v = 10:1):  $\delta$  (ppm) 13.17 (s, 4H, -NH), 8.28 (m, 1H, -OH), 7.60 (b, 8H,

-Ph), 7.53 (b, 2H, -Ph), 7.46 (b, 2H, -Ph), 7.25 (b, 8H, -Ph), 7.06 (b, 1H, -Ph), 6.86 (b, 2H, -Ph), 6.78 (b, 1H, -Ph), 5.72 (m, 4H, -Ph), 5.54 (b, 4H, -CH=C), 5.27 (s, 150H, -CH=CH- (Z)), 5.14 (s, 150H, -CH=CH- (E)), 4.90 (d, 4H, -CH=CH<sub>2</sub>), 4.79 (d, 4H, -CH=CH<sub>2</sub>), 3.94 (m, 3H, MeOH), 3.93 (m, 12H, -OMe), 3.36 (m, 8H, -CH<sub>2</sub>-C=C), 2.72 (s, 150H, -CH), 2.37 (s, 150H, -CH), 1.73 (m, 450H, -CH<sub>2</sub>), 1.28 (s, 300H, -CH<sub>2</sub>), 0.95 (m, 150H, -CH<sub>2</sub>).

For **Poly(NBE-2)** (400:1): Yield: 74%. FT-IR (KBr, cm<sup>-1</sup>): 3310 (b), 2941 (m), 2862 (s), 2735 (w), 2600 (m), 2534 (w), 2492 (w), 1990 (w), 1773 (m), 1713 (m), 1660 (w), 1614 (w), 1495 (s), 1447 (s), 1345 (m), 1255 (s), 1204 (m), 1149 (w), 1036 (s), 967 (vs), 910 (w), 865 (w), 818 (w), 747 (w), 674 (w), 580 (w), 493 (w), 431 (w).

For **Poly(NBE-3)** (200:1, 400:1, 600:1 or 800:1): Yield: 55% (200:1); 77% (400:1); 82% (600:1); 85% (800:1). FT-IR (KBr, cm<sup>-1</sup>): 3313 (b), 2945 (m), 2862 (s), 2734 (w), 2603 (m), 2530 (w), 2496 (w), 1994 (w), 1773 (m), 1710 (m), 1660 (w), 1616 (w), 1491 (s), 1448 (s), 1347 (m), 1257 (s), 1206 (m), 1145 (w), 1036 (s), 968 (vs), 912 (w), 864 (w), 820 (w), 743 (w), 670 (w), 580 (w), 497 (w), 438 (w).

For **Poly(NBE-4)** (400:1): Yield: 73%. FT-IR (KBr, cm<sup>-1</sup>): 3311 (b), 2943 (m), 2860 (s), 2733 (w), 2601 (m), 2530 (w), 2490 (w), 1994 (w), 1772 (m), 1711 (m), 1662 (w), 1616 (w), 1491 (s), 1448 (s), 1347 (m), 1257 (s), 1205 (m), 1148 (w), 1037 (s), 965 (vs), 912 (w), 864 (w), 820 (w), 745 (w), 671 (w), 582 (w), 497 (w), 438 (w).

### 3. Results and discussion

**Synthesis and characterization of the ligand HL and its series of complex monomers**

**{[Ln<sub>3</sub>(L)<sub>4</sub>Cl<sub>4</sub>(MeOH)(H<sub>2</sub>O)]·Cl} (Ln = La, 1; Ln = Eu, 2; Ln = Tb, 3 or Ln = Gd, 4)**

As shown in Scheme 1, 5-allyl-2-hydroxy-3-methoxy-benzaldehyde was synthesized by the Williamson synthesis and the subsequent *para* Claisen rearrangement with *o*-vanillin and allyl bromide as the starting materials in the presence of anhydrous K<sub>2</sub>CO<sub>3</sub> as the literature.<sup>17</sup> The diallyl-modified Salen-type Schiff-base precursor **H<sub>2</sub>L<sup>0</sup>** was obtained from the condensation reaction of *o*-phenylenediamine with 5-allyl-2-hydroxy-3-methoxy-benzaldehyde in a 1:2 molar ratio, while in refluxing absolute MeOH, the precursor **H<sub>2</sub>L<sup>0</sup>** was successfully converted into the off-white benzimidazole-type ligand **HL** in a good yield of 70%. Furthermore, reaction of the allyl-modified benzimidazole-type ligand **HL** and LnCl<sub>3</sub>·6H<sub>2</sub>O (Ln = La, Eu, Tb or Gd) in different metal to ligand molar ratios (1:1, 4:3 1:2 or 1:4) afforded the similar series of homo-leptic trinuclear complexes {[Ln<sub>3</sub>(L)<sub>4</sub>Cl<sub>4</sub>(MeOH)(H<sub>2</sub>O)]·Cl} (Ln = La, **1**; Ln = Eu, **2**; Ln = Tb, **3** or Ln = Gd, **4**), respectively, despite the slight difference of yields. Similar to the good solubility of the allyl-modified benzimidazole-type ligand **HL** in common organic solvents except for water, complexes **1-4** are also soluble in slightly-polar organic solvents due to the introduction of flexible allyl groups together with the charge of the two components (the cationic [Ln<sub>3</sub>(L)<sub>4</sub>Cl<sub>4</sub>(MeOH)(H<sub>2</sub>O)]<sup>+</sup> part and one free Cl<sup>-</sup> anion) in each of the four complexes.

[Scheme 1 inserted here]

The Schiff-base precursor **H<sub>2</sub>L<sup>0</sup>**, the benzimidazole-type ligand **HL** and its series of complexes **1-4** were well characterized by EA, FT-IR, <sup>1</sup>H NMR and ESI-MS. In the FT-IR spectra, two characteristic strong absorptions at 1620-1624 and 993-1000 cm<sup>-1</sup> attributed to the  $\nu$  vibration and the  $\omega$  vibration of the terminal active =CH<sub>2</sub> groups from allyl substituents were observed for the precursor **H<sub>2</sub>L<sup>0</sup>**, the ligand **HL** and complexes **1-4**, respectively. As to



the  $^1\text{H}$  NMR spectrum identification of the precursor  $\text{H}_2\text{L}^0$  or the ligand  $\text{HL}$ , the similar intra-molecular resonance-assisted hydrogen bonded (RAHB)  $\text{O-H}\cdots\text{N}$  proton resonance ( $\delta = 13.16$  ppm for  $\text{H}_2\text{L}^0$  or  $\delta = 11.09$  ppm for  $\text{HL}$ ) and the well-kept proton resonances ( $\delta = 6.01$ ,  $5.10$  and  $3.36$  ppm for  $\text{H}_2\text{L}^0$  or  $\delta = 6.09$ ,  $5.17$  and  $3.44$  ppm for  $\text{HL}$ ) of the functional allyl groups were exhibited. Nevertheless, the replacement of the typical  $-\text{CH}=\text{N}-$  proton resonance ( $\delta = 8.71$  ppm) for the precursor  $\text{H}_2\text{L}^0$  with the typical  $-\text{NH}$  proton resonance ( $\delta = 12.99$  ppm) for the ligand  $\text{HL}$  endowed their distinctive difference between. The  $^1\text{H}$  NMR spectrum (shown in Figure 1) of the *anti*-ferromagnetic trinuclear  $\text{La}_3$ -arrayed complex **1**, due to the coordination of  $\text{La}^{3+}$  ions, showed a slightly spread shift ( $\delta$  from  $13.17$  to  $3.33$  ppm) of the proton resonances of the ligands relative to that of the free ligand  $\text{HL}$  ( $\delta$  from  $12.99$  to  $3.44$  ppm). Moreover, besides the persistence of proton resonances ( $\delta = 6.03$ ,  $5.13$  and  $3.33$  ppm) for the terminal allyl groups of complex **1**, the presence of new proton resonances ( $\delta = 8.24$  and  $3.87$  ppm) from one coordinated  $\text{MeOH}$  molecule, together with the slight shift of the proton resonances of four coordinated ligands also confirmed the formation of  $\text{La}_3$ -arrayed complex **1**. The ESI-MS spectra of the series of complexes **1-4** displayed the similar patterns and exhibited the strong mass peak at  $m/z$   $1725.86$  (**1**),  $1765.02$  (**2**),  $1785.92$  (**3**) or  $1780.89$  (**4**) assigned to the major species of  $[\text{Ln}_3(\text{L})_4\text{Cl}_4(\text{MeOH})(\text{H}_2\text{O})]^+$  of complexes **1-4**, respectively. These observations further indicate that each of discrete homo-leptic  $\text{Ln}_3$ -arrayed units is retained in the corresponding dilute  $\text{MeCN}$  solution.

[Figure 1 inserted here]

The solid state structure of  $\text{3}\cdot 2\text{MeOH}\cdot 4\text{H}_2\text{O}$  as the representative of complexes **1-4** was determined by single-crystal X-ray diffraction analysis, and its crystallographic data and

selected bond parameters are presented in Tables 1 and 1S, respectively. Complex  $3 \cdot 2\text{MeOH} \cdot 4\text{H}_2\text{O}$  crystallizes in the triclinic space group  $P-1$ . For  $3 \cdot 2\text{MeOH} \cdot 4\text{H}_2\text{O}$ , the smallest symmetric unit is composed of one cation  $[\text{Tb}_3(\text{L})_4\text{Cl}_4(\text{MeOH})(\text{H}_2\text{O})]^+$ , one free  $\text{Cl}^-$  anion, two solvates  $\text{MeOH}$  and four solvates  $\text{H}_2\text{O}$ . As shown in Figure 2, four deprotonated ( $\text{L}^-$ ) ligands chelate to three  $\text{Tb}^{3+}$  ions with a non-linear linkage ( $\text{Tb1-Tb2-Tb3}$  angle of  $144.51(5)^\circ$ ), where the central  $\text{Tb}^{3+}$  ion ( $\text{Tb2}$ ) is bridged by two phenolic O atoms ( $\text{O1}$  and  $\text{O5}$  or  $\text{O3}$  and  $\text{O7}$ ) from the corresponding two deprotonated ( $\text{L}^-$ ) ligands to the two terminal  $\text{Tb}^{3+}$  ions ( $\text{Tb1}$  or  $\text{Tb3}$ ), respectively. The three  $\text{Tb}^{3+}$  ions exhibit three kinds of different coordination environments, where the unique central  $\text{Tb}^{3+}$  ion ( $\text{Tb2}$ ) is eight-coordinate and bound by two sets of the phenolic O atom ( $\text{O5}$  or  $\text{O7}$ ) and the methoxy O atom ( $\text{O6}$  or  $\text{O8}$ ) from two different deprotonated ( $\text{L}^-$ ) ligands and two sets of the imidazole N ( $\text{N2}$  or  $\text{N4}$ ) and the phenolic O atom ( $\text{O1}$  or  $\text{O3}$ ) from the other two different deprotonated ( $\text{L}^-$ ) ligands. However, both of the two terminal  $\text{Tb}^{3+}$  ions ( $\text{Tb1}$  and  $\text{Tb3}$ ) with the slightly different coordination environments are seven-coordinate: in addition to the imidazole N ( $\text{N6}$  or  $\text{N8}$ ) and the phenolic O atom ( $\text{O5}$  or  $\text{O7}$ ) from one deprotonated ( $\text{L}^-$ ) ligand and the phenolic O atom ( $\text{O1}$  or  $\text{O3}$ ) and the methoxy O atom ( $\text{O2}$  or  $\text{O4}$ ) from another deprotonated ( $\text{L}^-$ ) ligand, it saturate its coordination sphere from two coordinated  $\text{Cl}^-$  anions ( $\text{Cl1}$  and  $\text{Cl2}$  or  $\text{Cl3}$  and  $\text{Cl4}$ ) and one  $\text{O10}$  atom from the coordinated  $\text{H}_2\text{O}$  or one  $\text{O9}$  atom from the coordinated  $\text{MeOH}$  molecule, respectively. Two unique  $\text{Tb} \cdots \text{Tb}$  distances of  $3.8563(35)$  and  $3.8368(37)$  Å are between the central  $\text{Tb}^{3+}$  ion ( $\text{Tb2}$ ) and the two terminal  $\text{Tb}^{3+}$  ions ( $\text{Tb1}$  and  $\text{Tb3}$ ), respectively. In addition to the weak  $\text{N1-H1} \cdots \text{Cl5}$  H-bonding ( $3.045(2)$  Å, shown in Figure 1S) between the free  $\text{Cl}^-$  anion ( $\text{Cl5}$ ) for charge balance with one deprotonated ( $\text{L}^-$ ) ligand,

free solvates MeOH and H<sub>2</sub>O are not bound to the homo-leptic framework, and they exhibit no observed interactions with the host structure. It is worth noting that the homo-leptic trinuclear host structure in **3**·2MeOH·4H<sub>2</sub>O is distinctively different from the reported structures of mononuclear Ln-arrayed or homo-leptic binuclear Ln<sub>2</sub>-arrayed complexes<sup>23</sup> while comparable to Cl<sup>-</sup>-dependent homo-leptic Ln<sub>3</sub>-arrayed structure<sup>24</sup> based on the analogue Br-modified benzimidazole-type ligand. This result shows that the discrete homo-leptic Ln<sub>3</sub>-arrayed host structure of complex **3**·2MeOH·4H<sub>2</sub>O is stable and not strictly relied on the stoichiometries as the literature,<sup>23</sup> especially with the involvement of electron-donating allyl while not electron-withdrawing Br group. Moreover, all the four functional allyl groups with the C=C bond lengths of 1.297(10)-1.304(19) Å for the typical C=C bonds in complex **3**·2MeOH·4H<sub>2</sub>O are well retained.

[Figure 2 inserted here]

#### Photophysical property and energy transfer of the series of complexes $\{[Ln_3(L)_4Cl_4(MeOH)(H_2O)] \cdot Cl\}$ (Ln = Eu, **2**; Ln = Tb, **3** or Ln = Gd, **4**) in solution

The photophysical property of the ligand **HL** and its complexes **2-4** has been examined in dilute MeCN solution at RT or 77 K, and summarized in Table 2 and Figures 3-4. As shown in Figure 3, similar ligand-centered solution absorptions (224-226, 296-300 and 330-332 nm) of complexes **2-4** in the UV-visible region are observed, where all the intra-ligand low-energy  $\pi-\pi^*$  transition absorptions are red-shifted upon coordination of Ln<sup>3+</sup> ions compared to that (324 nm) of the free ligand **HL**. For complex **2**, photo excitation ( $\lambda_{ex}$  = 359 nm) of the chromophore just gives rise to weak residual visible emission ( $\lambda_{em}$  = 428 nm) assigned to the

$\pi$ - $\pi^*$  ligand transition, and no characteristic  $\text{Eu}^{3+}$ -based line-like emissions are observed. In contrast, for complex **3**, as shown in Figure 4, the ligand-centered emission is not detectable in the emission spectrum, while the strong characteristic ligand-field splitting emissions of  $\text{Tb}^{3+}$  ion from the emitting level ( $^5\text{D}_4$ ) to the ground multiple  $^7\text{F}_J$  ( $J = 6, 5, 4, 3$ ) are exhibited, respectively. The strongest emission ( $\lambda_{em} = 543 \text{ nm}$ ) based on the hyper-sensitive  $^5\text{D}_4 \rightarrow ^7\text{F}_5$  transition, together with the second maximum peak at 488 nm corresponding to the  $^5\text{D}_4 \rightarrow ^7\text{F}_6$  transition, endows the bright green solution luminescence with a CIE (Commission International De L'Eclairage) chromatic coordinate  $x = 0.304$  and  $y = 0.599$  for complex **3**.

[Figures 3-4 inserted here]

It is of special interest to explore the detailed mechanism of energy transfer process for the two complexes **2-3**. As a suitable reference compound, the  $\text{Gd}_3$ -arrayed complex **4** allows the further study of the chromophore luminescence in the absence of energy transfer, because the  $\text{Gd}^{3+}$  ion has no energy levels below  $32150 \text{ cm}^{-1}$ , and therefore cannot accept any energy from the excited state of the chromophore.<sup>25</sup> Different from the typical fluorescence ( $\lambda_{em} = 426$  and  $\tau = 1.51 \text{ ns}$ ) at RT, as shown in Figure 2S, complex **4** exhibits the phosphorescence ( $\lambda_{em} = 433$  and  $\tau = 29.4 \mu\text{s}$ ) at 77 K, from which the triplet ( $^3\pi$ - $\pi^*$ ) energy level at  $23095 \text{ cm}^{-1}$  is obtained. With regard to the singlet ( $^1\pi$ - $\pi^*$ ) energy level ( $28736 \text{ cm}^{-1}$ ) estimated by the lower wavelength of its UV-visible absorbance edge, so the larger energy gap  $\Delta E_1$  ( $5641 \text{ cm}^{-1}$ ,  $^1\pi$ - $\pi^* - ^3\pi$ - $\pi^*$ ) than  $5000 \text{ cm}^{-1}$ , as shown in Figure 5, endows the effective inter-system crossing process according to Reinholdt's empirical rule.<sup>26</sup> Further through checking the energy level match between the ligand-based  $^3\pi$ - $\pi^*$  energy level ( $23095 \text{ cm}^{-1}$ ) and the first excited state level of  $\text{Eu}^{3+}$  or  $\text{Tb}^{3+}$  ion, in spite of the energy gap ( $\Delta E_2 = 5809 \text{ nm}$ ) for complex

2, it is actually large enough to go beyond the reasonable range of 2500-4000  $\text{cm}^{-1}$  from Latva's empirical rule.<sup>27</sup> The possible heavy non-radiative deactivation results in the complete quenching of the characteristic  $\text{Eu}^{3+}$ -based emissions. As to complex **3**, the relatively smaller energy gap ( $\Delta E_2 = 2550 \text{ nm}$ ) within the ideal 2500-4500  $\text{cm}^{-1}$  range<sup>27</sup> confirms the suitability of the allyl-modified benzimidazole-type ligand **HL** as a sensitizer for  $\text{Tb}^{3+}$  ion. The  $\text{Tb}^{3+}$  ion ( $^5\text{D}_4$ ) lifetime of complex **3** (Figure 6) under excitation of 346 nm is measured to be  $\tau_{\text{obs}} = 104.54 \mu\text{s}$ , which is not one of the longest so far reported  $\text{Tb}^{3+}$ -complexes,<sup>28</sup> while the attractive high quantum yield ( $\Phi_{\text{overall}}$ , 72%) for complex **3** in solution is obtained. This should be mainly attributed to the suitable energy level match and the additive electronic communication between three  $\text{Tb}^{3+}$  centers in complex **3** despite the vibrational quenching<sup>7</sup> from OH-containing oscillators (MeOH and  $\text{H}_2\text{O}$ ) in the inner coordination spheres of the two terminal  $\text{Tb}^{3+}$  ions.

[Figures 5-6 inserted here]

#### Synthesis and characterization of PMMA-supported doping hybrid materials **1@PMMA**, **2@PMMA**, **3@PMMA** and **4@PMMA** and PNBE-supported metallopolymer-type hybrid materials **Poly(NBE-1)**, **Poly(NBE-2)**, **Poly(NBE-3)** and **Poly(NBE-4)**

In consideration of the excellent performance of PMMA as one of the popular polymer matrices with low cost, low optical absorbance and good mechanical property,<sup>29</sup> it is of interest to explore the radical polymerization behaviors of the series of  $\text{Ln}_3$ -arrayed complexes **1-4** containing four active allyl groups as the complex monomers like those<sup>16</sup>

containing active vinyl groups with MMA in activation with AIBN. To our dismay, the copolymerization does not effectively occur as expected, where each of complexes **1-4** is just physically doped into the *in situ* formed PMMA matrix from homo-polymerization of MMA, exclusively giving the series of PMMA-supported doping hybrid materials **1@PMMA**, **2@PMMA**, **3@PMMA** and **4@PMMA**, as shown in Scheme 2, respectively. As to the isolated hybrid materials, in the FT-IR spectra from the simple combination of characteristic absorptions from each of **1-4** and PMMA, the intense absorption band at 1731-1732 cm<sup>-1</sup> attributed to the  $\nu(\text{C=O})$  vibration of PMMA appears, and the characteristic absorptions at 1621-1625 and 1000-1002 cm<sup>-1</sup> assigned to the  $\nu(\text{allyl})$  vibration and the  $\omega(\text{allyl})$  vibration of complexes **1-4** are weakened while well kept due to the low concentration doping. Nevertheless, the absence of the band absorptions in the range of 3373-3390 cm<sup>-1</sup> attributed to the coordinated MeOH and H<sub>2</sub>O in complexes **1-4**, together with the slight blue-shift by 3-4 cm<sup>-1</sup> of  $\nu(\text{C=O})$  vibrations (1731-1732 cm<sup>-1</sup>) of **1@PMMA**, **2@PMMA**, **3@PMMA** and **4@PMMA** than that (1728 cm<sup>-1</sup>) of pure PMMA indicates that the two coordinated MeOH and H<sub>2</sub>O should be replaced by carbonyl groups from PMMA through physical doping (also shown in Scheme 2). Especially based on the <sup>1</sup>H NMR spectrum (also shown in Figure 1) of *anti*-ferromagnetic **1@PMMA**, the well combined and almost no shifted proton resonances of the coordinated benzimidazole-type ligand (**L**)<sup>-</sup> and PMMA are unambiguously identical to those of complex **1** and PMMA, respectively. The results indicate that the series of complexes **1-4** with active allyl groups can not be copolymerized with MMA in presence of AIBN through the free-radical mechanism,<sup>16</sup> probably due to the degradative chain transfer<sup>30</sup> of the flexible allyl groups, from which lower reactivity of the resonance-stabilized monomeric

radical formed from those complex monomers than that of MMA leads much less tendency to initiate a new polymer chain. It is of special notice that the quantitative  $^1\text{H}$  NMR analysis of **1@PMMA** further shows the distinctively lower molar ratio of 110:1 than the initial feed molar ratio (400:1) of MMA with **1**, which should be due to the loss of MMA from oligometric PMMA.

[Scheme 2 inserted here]

Assisted by the success of homo-polymerization of NBE or its derivatives<sup>31</sup> and their copolymerization<sup>17,32</sup> with many other C=C-containing (including allyl groups) functional monomers using the typical ROMP in activation with Grubbs-type catalysts, the copolymerization of the series of  $\text{Ln}_3$ -arrayed complexes **1-4** containing four active allyl groups with NBE were carried out in absolute  $\text{CHCl}_3$  at RT in activation with H-Grubbs II (also in Scheme 2). Undoubtedly, all the copolymerizations were complete after 72 h as expected, from which each of the benzimidazole-based  $\text{Ln}_3$ -arrayed unit with four functional allyl groups is covalently bonded to the PNBE polymeric backbone, thus the first example of metallopolymer based on the homo-trinuclear  $\text{Ln}_3$ -arrayed units is constructed to date. The isolated metallopolymer-type hybrid materials **Poly(NBE-1)**, **Poly(NBE-2)**, **Poly(NBE-3)** and **Poly(NBE-4)** with Wolf Type II fashion<sup>33</sup> are also well characterized by FT-IR,  $^1\text{H}$  NMR and GPC. In the FT-IR spectra, the characteristic absorptions of unsaturated C=C bonds from allyl groups of complexes **1-4** completely disappear. The  $^1\text{H}$  NMR spectrum analysis of the *anti*-ferromagnetic **Poly(NBE-1)** (also shown in Figure 1) shows the combined proton resonances ( $\delta = 13.17$  to 0.95 ppm) of the coordinated benzimidazole-type ligand (**L**)<sup>+</sup> and NBE, where the proton resonances of new -CH=CH- within at 5.54 ppm and the terminal

-C=CH<sub>2</sub> at 4.90 and 4.79 ppm from NBE-ring-opening groups of **1**, together with those of the *Z*-mode -CH=CH- at 5.27 ppm and the *E*-mode -CH=CH- at 5.14 ppm from PNBE, are displayed, respectively. As shown in Table 2S, the number-average molecular weights ( $M_n$ ) and polydispersity indexes ( $PDI = M_w/M_n$ ) of the series of PNBE-supported grafting hybrid materials from different feeding molar ratios are in the range of 20020-25592 g/mol and 2.11-2.58, respectively, where those relatively lower molecular weights in the 10<sup>4</sup> g/mol magnitude could endow the good solubility and the facilitated film-forming. Especially for the obtained hybrid materials **Poly(NBE-3)** from different feeding molar ratios (200:1, 400:1, 600:1 and 800:1) with NBE to **3**, there has an almost linear relationship between the molecular weights and the feeding molar ratios, suggesting a random-bonding while homogeneous distribution of **3** along the polymeric backbone.<sup>34</sup>

PXRD patterns of the two series of {[Ln<sub>3</sub>(L)<sub>4</sub>Cl<sub>4</sub>(MeOH)(H<sub>2</sub>O)]·Cl}-containing doping and grafting hybrid materials (as shown in Figures 7a and 7b) show only amorphous peaks of PMMA and PNBE, respectively. It suggests that in the two kinds of hybrid materials with the good film-forming property, the Ln<sub>3</sub>-arrayed benzimidazole-type complex unit is homogeneously distributed into the PMMA matrix with complicated weak interactions or the PNBE matrix with strong covalently-bonds between, respectively, especially on the condition of low concentrations. Moreover, TG analysis of the series of PMMA-supported doping hybrid materials shows an increase of about 25 °C for the  $T_{onset}$  in comparison with the pure PMMA, as shown in Figure 8, and a relatively slight increase (15 °C) is observed for another series of PNBE-supported metallopolymer-type hybrid materials as compared with pure PNBE. However, the decomposition with maxima around much higher temperature interval



(452-458 °C) for the PNBE-supported metallopolymer-type hybrid materials than that (366-372 °C) for the PMMA-supported doping hybrid materials is exhibited, and both are distinctively higher than that (278 °C) of the representative complex **3**. These observations further demonstrate that the thermal stabilities of the two kinds of hybrid materials are essentially improved by doping or grafting, and the metallopolymer-type hybrid materials are more stable in relative to those physical doping hybrid materials.

[Figures 7 and 8 inserted here]

**Photophysical properties of the two series of hybrid materials **2@PMMA**, **3@PMMA** and **4@PMMA** and Poly(NBE-2), Poly(NBE-3) and Poly(NBE-4) in solid state**

For the two series of hybrid materials, their photophysical properties in solid state at RT or 77 K have been examined, and also summarized in Table 2 and Figures 9-12 and 2S. As shown in Figure 9, the DR spectra of both the PMMA-supported doping and PNBE-supported metallopolymer-type hybrid materials from complexes **2-4** exhibit the relatively broader absorption bands than those of complexes **2-4** in solution, where the absorptions at 212-214, 298-304 and 347-350 nm or 208-210, 222-224, 303-304 and 341-344 nm in the UV-visible region should be assigned to electronic transitions from the organic moieties of both the coordinated benzimidazole-type ligands and PMMA or PNBE, respectively. Due to the characteristic absorption bands of  $\text{Eu}^{3+}$ ,  $\text{Tb}^{3+}$  or  $\text{Gd}^{3+}$  ion commonly appearing above 1000 nm,<sup>35</sup> they are not discerned in the corresponding samples. Upon excitation of the chromophore's absorption band ( $\lambda_{\text{ex}} = 346$  nm for **2@PMMA** or  $\lambda_{\text{ex}} = 343$  nm for **4@PMMA**), both **2@PMMA** and **4@PMMA** in solid state also exhibit the ligand-based

emissions shown in Figure 10, and **3@PMMA** also gives rise to the strong characteristic ligand-field splitting while also high color-purity green emissions ( $^5D_4 \rightarrow ^7F_J$ ,  $J = 6, 5, 4, 3$  shown in Figure 11a and a CIE coordinate of  $x = 0.302$  and  $y = 0.598$  shown in Figure 12) of  $Tb^{3+}$  ion. Especially for the solid **3@PMMA**, the lifetime value ( $\tau = 291.50 \mu s$  also shown in Figure 6) is found to distinctively increase in relative to that of complex **3** in solution, which should be assigned to the newly coupling interactions between  $-C=O$  of PMMA with the OH-containing oscillators around  $Tb^{3+}$  ions to suppress the multiphonon relaxation.<sup>36</sup> Similarly, for the PNBE-supported metallopolymer-type hybrid material **Poly(NBE-3)**, the ligand-centered emission is also completely quenched, and the stronger high color-purity green emission with a CIE coordinate of  $x = 0.301$  and  $y = 0.600$  (also shown in Figure 12) of  $Tb^{3+}$  ion is observed, as shown in Figure 11b.

[Figures 9-12 inserted here]

It is worth noting that the maximum excitation positions ( $\lambda_{ex} = 383$  nm for **Poly(NBE-2)**,  $\lambda_{ex} = 395$  nm for **Poly(NBE-3)** or  $\lambda_{ex} = 381$  nm for **Poly(NBE-4)**) for the PNBE-supported grafting hybrid materials in solid state are all distinctively red-shifted as compared to the solution spectra of complex monomers **2-4** or the solid spectra of the PMMA-supported doping hybrid materials. This result, together with the slight red-shift of the ligand-centered emission for **Poly(NBE-2)** or **Poly(NBE-4)**, suggests the increased conjugation from the formation of covalently-bonded metallopolymer.<sup>37</sup> Moreover, the extension of the PNBE-based backbone for **Poly(NBE-3)**, changes the ligand electric fields around the  $Tb^{3+}$  ions, leading to the further increase of lifetime value ( $\tau = 451.04 \mu s$  also shown in Figure 6). From the viewpoint of energy transfer, the weak coupling interactions in **3@PMMA** or the

strong covalently-bonding in **Poly(NBE-3)** probably could recombine the charge carrier at Tb<sup>3+</sup>-related trap site<sup>35</sup> in the corresponding polymer matrix, endowing the effective decrease of the <sup>3</sup>π-π\* energy level (22222 cm<sup>-1</sup> or 21978 cm<sup>-1</sup>) of the chromophore to strengthen the ligands-to-metal energy transfer. These results based on more suitable energy match (also shown in Figure 5) are well in accordance with the relatively larger quantum yields ( $\Phi_{\text{overall}}$ , 76% for **3@PMMA** or 83% for **Poly(NBE-3)**). Noticeably, the emission spectra of both **3@PMMA** ( $\lambda_{\text{ex}} = 370$  nm) and **Poly(NBE-3)** ( $\lambda_{\text{ex}} = 395$  nm) from the Tb<sub>3</sub>-arrayed complex **3** at a variety of feeding molar ratios (200:1, 400:1, 600:1 and 800:1), exhibit the same well-defined emission peaks characteristic of the <sup>5</sup>D<sub>4</sub> → <sup>7</sup>F<sub>J</sub> (J = 6, 5, 4, 3) transitions of Tb<sup>3+</sup> ion, as shown in Figure 11. Although there has an almost linear relationship between the hyper-sensitive emission intensity and the feeding molar ratio, the concentration self-quenching<sup>36</sup> for the series of doping hybrid materials **3@PMMA** at 400:1 is effectively prevented from the formation of uniform grafting hybrid materials **Poly(NBE-3)**.

#### 4. Conclusion

Through the self-assembly from the allyl-modified benzimidazole-type ligand **HL** and LnCl<sub>3</sub>·6H<sub>2</sub>O, a series of homo-leptic Ln<sub>3</sub>-arrayed complexes {[Ln<sub>3</sub>(L)<sub>4</sub>Cl<sub>4</sub>(MeOH)(H<sub>2</sub>O)]·Cl} (Ln = La, **1**; Ln = Eu, **2**; Ln = Tb, **3** or Ln = Gd, **4**) are obtained, respectively, in which energy transfer mechanism reveals the suitable energy level match for the Tb<sub>3</sub>-arrayed complex **3** with efficient green luminescence ( $\Phi_{\text{overall}} = 72\%$ ). Moreover, each of these complex monomers **1-4** cannot be copolymerized with MMA from the radical polymerization, while can be effectively copolymerized with NBE through ROMP, giving two kinds of

PMMA-supported doping hybrid materials **1@PMMA**, **2@PMMA**, **3@PMMA** and **4@PMMA** and PNBE-supported metallopolymer-type hybrid materials **Poly(NBE-1)**, **Poly(NBE-2)**, **Poly(NBE-3)** and **Poly(NBE-4)** respectively. For both **3@PMMA** and **Poly(NBE-3)** with high color-purity characteristic emissions of  $\text{Tb}^{3+}$  ion, the significantly improved physical properties, such as thermal stability, film-forming property and the luminescent property, are exhibited, and the covalently-bonding endows the higher-concentration (up to 400:1) self-quenching. This result suggests that these hybrid materials especially the metallopolymer-type hybrid materials can be used as green luminescent optical fibers for practical applications of high color-purity polymer-based OLEDs.

### Supporting information

The synthesis and characterization of **PMMA** in activation with AIBN and **PNBE** in activation with H-Grubbs II in Supporting information; the selected bond lengths (Å) and bond angles (°) for **3**·2MeOH·4H<sub>2</sub>O and GPC data of the samples of **PMMA**, **PNBE** and the series of metallopolymer **Poly(NBE-1)**, **Poly(NBE-2)**, **Poly(NBE-3)** and **Poly(NBE-4)** in Tables 1-2S; Perspective drawing of the weak N1-H1...Cl5 H-bonding (3.045(2) Å) interaction between the host framework and the free Cl5 in complex **3**·2MeOH·4H<sub>2</sub>O and the visible emission and excitation spectra of complex **4** in MeCN solution at  $1 \times 10^{-5}$  M and the hybrid materials **4@PMMA** and **Poly(NBE-4)** with the feeding molar ratio of 400:1 in solid state at 77 K in Figures 1-2S, respectively.

## Acknowledgements

This work is funded by the National Natural Science Foundation (21373160, 91222201, 21173165), the Program for New Century Excellent Talents in University from the Ministry of Education of China (NCET-10-0936), the research fund for the Doctoral Program (20116101110003) of Higher Education, the Science and Technology and Innovation Project (2012KTCQ01-37) of Shaanxi Province, Graduate Innovation and Creativity Fund (Visiting Learner) of Northwest University in P. R. of China.

## References

- 1 (a) J. Kido and Y. Okamoto, *Chem. Rev.*, 2002, **102**, 2357; (b) M. A. Katkova and M. N. Bochkarev, *Dalton Trans.*, 2010, **39**, 6599.
- 2 (a) S. Sivakumar, F. C. J. M. Van Veggel and M. Raudsepp, *J. Am. Chem. Soc.*, 2005, **127**, 12464; (b) Q.-L. Dai, M. E. Foley, C. J. Breshike, A. Lita, S. Adrian and G. F. Strouse, *J. Am. Chem. Soc.*, 2011, **133**, 15475; (c) M. M. Shang, C. X. Li and J. Lin, *Chem. Soc. Rev.*, 2014, **43**, 1372.
- 3 (a) F. Wang, Y. Han, C. S. Lim, Y. H. Lu, J. Wang, J. Xu, H. Y. Chen, C. Zhang, M. H. Hong and X. G. Liu, *Nature*, 2010, **463**, 1061; (b) L. Armelao, S. Quici, F. Barigelletti, G. Accorsi, G. Bottaro, M. Cavazzini and E. Tondello, *Coord. Chem. Rev.*, 2010, **254**, 487; (c) S. Roy, A. Chakraborty and T. K. Maji, *Coord. Chem. Rev.*, 2014, **273-274**, 139; (d) T. W. Duan and B. Yan, *J. Mater. Chem. C*, 2014, **2**, 5098.
- 4 (a) J.-C. G. Bünzli, *Chem. Rev.*, 2010, **110**, 2729; (b) X. H. Wang, H. B. Chang, J. Xie, B. Z. Zhao, B. T. Liu, S. L. Xu, W. B. Pei, N. Ren, L. Huang and W. Huang, *Coord. Chem. Rev.*,

- 273-274**, 201; (c) M. C. Heffem, L. M. Matosziuk and T. J. Meade, *Chem. Rev.*, 2014, **114**, 4496.
- 5 E. G. Moore, A. P. S. Samuel and K. N. Raymond, *Acc. Chem. Res.*, 2009, **42**, 542.
- 6 P. A. Tanner and C.-K. Duan, *Coord. Chem. Rev.*, 2010, **254**, 3026.
- 7 J.-C. G. Bünzli and S. V. Eliseeva, in *Springer Series on Fluorescence, Vol. 7, Lanthanide Spectroscopy, Materials, and Bio-applications*, ed. P. Hänninen and H. Härmä, Springer Verlag, Berlin, Germany, 2010, vol. 7, ch. 2.
- 8 (a) B. Yan, *RSC Adv.*, 2012, **2**, 9304; (b) L. D. Carlos, R. A. S. Ferreira, V. De Zea Bermudez, B. Julian-Lopez and P. Escribano, *Chem. Soc. Rev.*, 2011, **40**, 536.
- 9 K. Binnemans, *Chem. Rev.*, 2009, **109**, 4283.
- 10 J. Feng and H. J. Zhang, *Chem. Soc. Rev.*, 2013, **42**, 387;
- 11 J. M. Stanley and B. J. Holliday, *Coord. Chem. Rev.*, 2012, **256**, 1520.
- 12 (a) J. Pei, X. L. Liu, W. L. Yu, Y. H. Lai, Y. H. Liu and R. Cao, *Macromolecules*, 2002, **35**, 7274; (b) A. Balamurugan, M. L. P. Reddy and M. Jayakannan, *J. Phys. Chem. B*, 2009, **113**, 14128.
- 13 A. Meyers, A. Kimyonok and M. Weck, *Macromolecules*, 2005, **38**, 8671.
- 14 (a) Q. Ling, Y. Song, S. J. Ding, C. Zhu, D. S. H. Chan, D.-L. Kwong, E.-T. Kang and K.-G. Neoh, *Adv. Mater.*, 2005, **17**, 455; (b) H. Xu, R. Zhu, P. Zhao and W. Huang, *J. Phys. Chem. C*, 2011, **115**, 15627.
- 15 X. Y. Chen, X. P. Yang and B. J. Holliday, *J. Am. Chem. Soc.*, 2008, **130**, 1546.
- 16 (a) J. F. Li, F. Y. Song, L. Wang, J. M. Jiao, Y. X. Cheng and C. J. Zhu, *Macromol. Rapid Commun.*, 2012, **33**, 1268; (b) Z. Zhang, W. X. Feng, P. Y. Su, X. Q. Lü, J. R. Song, D. D.

- Fan, W.-K. Wong, R. A. Jones and C. Y. Su, *Inorg. Chem.*, 2014, **53**, 5950; (c) Z. Zhang, W. X. Feng, P. Y. Su, L. Liu, X. Q. Lü, J. R. Song, D. D. Fan, W.-K. Wong, R. A. Jones and C. Y. Su, *Synthe. Metals*, 2015, **199**, 128; (d) T. Z. Miao, W. X. Feng, Z. Zhang, P. Y. Su, X. Q. Lü, J. R. Song, D. D. Fan, W.-K. Wong, R. A. Jones and C.-Y. Su, *Eur. J. Inorg. Chem.*, 2014, 2839.
- 17 W. X. Feng, Y. Zhang, Z. Zhang, P. Y. Su, X. Q. Lü, J. R. Song, D. D. Fan, W.-K. Wong, R. A. Jones and C. Y. Su, *J. Mater. Chem. C*, 2014, **2**, 1489.
- 18 S. Comby and J. -C. G. Bünzli, in *Handbook on the Physics and Chemistry of Rare Earths*, ed. Jr K. A. Gschneidner, J.-C. G. Bünzli and V. K. Pecharsky, Elsevier Science B. V., Amsterdam, The Netherlands, 2007, vol. 37, ch. 235.
- 19 (a) C. de Mello Donegá, S. Alves and G. F. De Sá Jr., *Chem. Commun.*, 1996, **10**, 1199; (b) J. C. de Mello, H. F. Wittmann and R. H. Friend, *Adv. Mater.*, 1997, **9**, 230.
- 20 G. M. Sheldrick, *SHELXL-97: Program for crystal structure refinement*, Göttingen, Germany, 1997.
- 21 G. M. Sheldrick, *SADABS*, University of Göttingen, Germany, 1996.
- 22 W. A. Braunecker and K. Matyjaszewski, *Prog. Polym. Sci.*, 2007, **32**, 93.
- 23 X. P. Yang, R. A. Jones, M. M. Oye, M. J. Wiester and R. J. Lai, *New J. Chem.*, 2011, **35**, 310.
- 24 X. P. Yang, R. A. Jones, M. J. Wiester, M. M. Oye and W.-K. Wong, *Cryst. Growth & Des.*, 2010, **10**, 970.
- 25 W. T. Carnall, P. R. Fields and K. Rajnak, *J. Chem. Phys.*, 1968, **49**, 4443.
- 26 F. J. Steemers, W. Verboom, D. N. Reinhoudt, E. B. van der Tol and J. W. Verhoeven, *J.*

- Am. Chem. Soc.*, 1995, **117**, 9408.
- 27 M. Latva, H. Takalo, V. M. Mukkala, C. Matachescu, J. C. Rodriguez-Ubis and J. Kanakare, *J. Lumin.*, 1997, **75**, 149.
- 28 L. J. Xu, G. T. Xu and Z. N. Chen, *Coord. Chem. Rev.*, 2014, **273-274**, 47.
- 29 (a) K. Lunstroot, K. Driesen, P. Nockemann, L. Viau, P. H. Mutin, A. Vioux and L. Binnemans, *Phys. Chem. Chem. Phys.*, 2010, **12**, 1879; (b) W. Q. Fan, J. Feng, S. Y. Song, Y. Q. Lei, G. L. Zheng and H. J. Zhang, *Chem. Eur. J.*, 2010, **16**, 1903; (c) S. Sivakumar and M. L. P. Reddy, *J. Mater. Chem.*, 2012, **22**, 10852; (d) S. Biju, Y. K. Eom, J.-C. G. Bünzli and H. K. Kim, *J. Mater. Chem. C*, 2013, **1**, 6935.
- 30 S. Inoue, T. Kumagai, H. Tamezawa, H. Aota, A. Matsumoto, K. Yokoyama, Y. Matoba and M. Shibano, *J. Polym. Sci. A*, 2011, **49**, 156.
- 31 W. J. Sommer and M. Weck, *Coord. Chem. Rev.*, 2007, **151**, 860.
- 32 S. K. Yang, A. V. Ambade and M. Weck, *Chem. Soc. Rev.*, 2011, **40**, 129.
- 33 M. O. Wolf, *Adv. Mater.*, 2001, **13**, 545.
- 34 P. Gumbley, D. Koylu and S. W. Thomas, *Macromolecules*, 2011, **44**, 7956.
- 35 F. Mercier, C. Alliot, L. Bion, N. Thromat and P. Toulhoat, *J. Electron Spectrosc. Relat. Phenom.*, 2006, **150**, 21.
- 36 H. X. Huang, J. Liu and Y. Q. Cai, *J. Lumin.*, 2013, **143**, 447.
- 37 J. Feng, J. B. Yu, S. Y. Song, L. N. Sun, W. Q. Fan, X. M. Guo, S. Dang and H. J. Zhang, *Dalton Tran.*, 2009, 2406.
- 38 P. Martin-Ramos, V. Lavín, M. Ramos Silva, I. R. Martín, F. Lahoz, P. Chamorro-Posada, J. A. Paixão and J. Martín-Gil, *J. Mater. Chem. C*, 2013, **1**, 5701.



39 L. D. Carlos, R. A. S. Ferreira, V. de Z. Bermudez, B. Julian-Lopez and P. Escribano,

*Chem. Soc. Rev.*, 2011, **40**, 536.

**Table 1** Crystal data and structure refinement for complex **3**·2MeOH·4H<sub>2</sub>O

Compound	<b>3</b> ·2MeOH·4H <sub>2</sub> O
Empirical formula	C <sub>71</sub> H <sub>82</sub> Cl <sub>5</sub> N <sub>8</sub> O <sub>16</sub> Tb <sub>3</sub>
Formula weight	1957.46
Crystal size/mm	0.26 × 0.23 × 0.21
<i>T</i> /K	296(2)
$\lambda$ /Å	0.71073
Crystal system	Triclinic
Space group	<i>P</i> -1
<i>a</i> /Å	16.089(15)
<i>b</i> /Å	17.155(17)
<i>c</i> /Å	18.684(17)
$\alpha$ /°	71.523(16)
$\beta$ /°	80.787(19)
$\gamma$ /°	62.199(15)
<i>V</i> /Å <sup>3</sup>	4326(7)
<i>Z</i>	2
$\rho$ /g·cm <sup>-3</sup>	1.503
$\mu$ /mm <sup>-1</sup>	2.641
<i>F</i> (000)	1944
Data/restraints/parameters	15042/53/908
Quality-of-fit indicator	0.976
Final <i>R</i> indices [ <i>I</i> > 2σ( <i>I</i> )]	<i>R</i> <sub>1</sub> = 0.0975 <i>wR</i> <sub>2</sub> = 0.2480
<i>R</i> indices (all data)	<i>R</i> <sub>1</sub> = 0.1798 <i>wR</i> <sub>2</sub> = 0.3223

**Table 2** The photophysical properties of the ligand **HL** and its complexes **2-4** at  $1 \times 10^{-5}$  M in absolute MeCN solution, the PMMA-supported doping hybrid materials **2@PMMA**, **3@PMMA** and **4@PMMA**, the PNBE-supported metallopolymer-type hybrid materials **Poly(NBE-2)**, **Poly(NBE-3)** and **Poly(NBE-4)** from the same feeding molar ratio of 400:1 in solid state at RT or 77 K

Compound	Absorption	Excitation	Emission		
	$\lambda_{ab}/nm$ [ $\log(\epsilon/dm^3 mol^{-1} cm^{-1})$ ]	$\lambda_{ex}/nm$	$\lambda_{em}/nm$	$\tau$	$\Phi$
<b>HL</b>	228 (0.57), 300 (0.53), 324(0.36)	326	405(s)	1.67 ns	- <sup>a</sup>
<b>2</b> (Ln <sup>3+</sup> = Eu <sup>3+</sup> )	226(1.55), 298(0.97), 330(0.59)	272, 317, 359	428(w)	< 1 ns	< 10 <sup>-5</sup>
<b>3</b> (Ln <sup>3+</sup> = Tb <sup>3+</sup> )	226(1.61), 296(0.95), 332(0.58)	273, 346	488, 543, 583, 622	104.54 $\mu s$	0.72
<b>4</b> (Ln <sup>3+</sup> = Gd <sup>3+</sup> )	224(1.75), 300(1.00), 330(0.61)	274, 317, 359	426(m)	1.51 ns	- <sup>a</sup>
		272, 318, 359	433(s)	29.4 $\mu s$ (77 K)	- <sup>a</sup>
<b>2@PMMA</b>	212, 304, 347	282(sh), 346	430(w)	- <sup>a</sup>	- <sup>a</sup>
<b>3@PMMA</b>	214, 298, 350	303, 370	492, 548, 588, 623	291.50 $\mu s$	0.76
<b>4@PMMA</b>	212, 304, 348	281(sh), 343	426(m)	1.38 ns	- <sup>a</sup>
		304, 361	450(s)	89.0 $\mu s$ (77 K)	- <sup>a</sup>
<b>Poly(NBE-2)</b>	208, 222, 304, 341	320, 383	443(w)	- <sup>a</sup>	- <sup>a</sup>
<b>Poly(NBE-3)</b>	210, 223, 304, 342	325, 395	491, 547, 586, 624	451.04 $\mu s$	0.83
<b>Poly(NBE-4)</b>	209, 224, 303, 344	318, 381	440(m)	0.92 ns	- <sup>a</sup>
		317, 383	455(s)	174.8 $\mu s$ (77 K)	- <sup>a</sup>

<sup>a</sup>The lifetime or the quantum yield of the emission is too weak or unnecessary to be determined.

## Captions to Schemes and Figures

**Scheme 1** Reaction scheme for the synthesis of the diallyl-modified Salen-type Schiff-base precursor  $\text{H}_2\text{L}^0$ , the allyl-modified benzimidazole-type ligand **HL** and its series of homo-leptic  $\text{Ln}_3$ -arrayed complexes **1-4**.

**Scheme 2** Reaction scheme for the synthesis of PMMA-supported doping hybrid materials **1@PMMA**, **2@PMMA**, **3@PMMA** and **4@PMMA** and PNBE-supported metallopolymer-type hybrid materials **Poly(NBE-1)**, **Poly(NBE-2)**, **Poly(NBE-3)** and **Poly(NBE-4)**.

**Figure 1**  $^1\text{H}$  NMR spectra for **PMMA**, **PNBE**, **1**, **1@PMMA** and **Poly(NBE-1)** from the feeding molar ratio of 400:1 in  $\text{DMSO}-d_6$  and/or  $\text{CDCl}_3$  at RT.

**Figure 2** Perspective drawing of the cationic part in complex **3**·2MeOH·4H<sub>2</sub>O; H atoms, free anion  $\text{Cl}^-$  and solvates are omitted for clarity.

**Figure 3** UV-visible absorption spectra of the allyl-modified benzimidazole-type ligand **HL** and its  $\text{Ln}_3$ -arrayed complexes **2-4** in MeCN solution at  $1 \times 10^{-5}$  M at RT.

**Figure 4** Visible emission and excitation spectra of the ligand **HL** and its complexes **2-4** in MeCN solution at  $1 \times 10^{-5}$  M at RT.

**Figure 5** Schematic energy level diagram and energy transfer process of  $\text{Eu}^{3+}$  or  $\text{Tb}^{3+}$  for complex **2-3** in solution and the PMMA-supported doping or PNBE-supported metallopolymer-type hybrid materials based on complexes **2-3** with the same feeding molar ratio of 400:1 in solid state.

**Figure 6** Luminescence decay profiles for complex **3** in solution and the hybrid materials **3@PMMA** and **Poly(NBE-3)** from the same feeding molar ratio of 400:1 in solid state with emission monitored at approximate 545 nm.

**Figure 7** PXRD patterns of PMMA and its series of PMMA-supported doping hybrid materials **2@PMMA**, **3@PMMA** and **4@PMMA** (7a), PNBE and its series of PNBE-supported metallopolymer-type hybrid materials **Poly(NBE-2)**, **Poly(NBE-3)** and **Poly(NBE-4)** (7b) from the same feeding molar ratio of 400:1 in solid state.

**Figure 8** TG curves of complex **3**, PMMA, PNBE, and the two series of PMMA-supported doping hybrid materials **2@PMMA**, **3@PMMA** and **4@PMMA** and PNBE-supported metallopolymer-type hybrid materials **Poly(NBE-2)**, **Poly(NBE-3)** and **Poly(NBE-4)** from the same feeding molar ratio of 400:1 in solid state.

**Figure 9** DR spectra of the two series of PMMA-supported doping hybrid materials **2@PMMA**, **3@PMMA** and **4@PMMA** and PNBE-supported metallopolymer-type hybrid materials **Poly(NBE-2)**, **Poly(NBE-3)** and **Poly(NBE-4)** from the same feeding molar ratio of

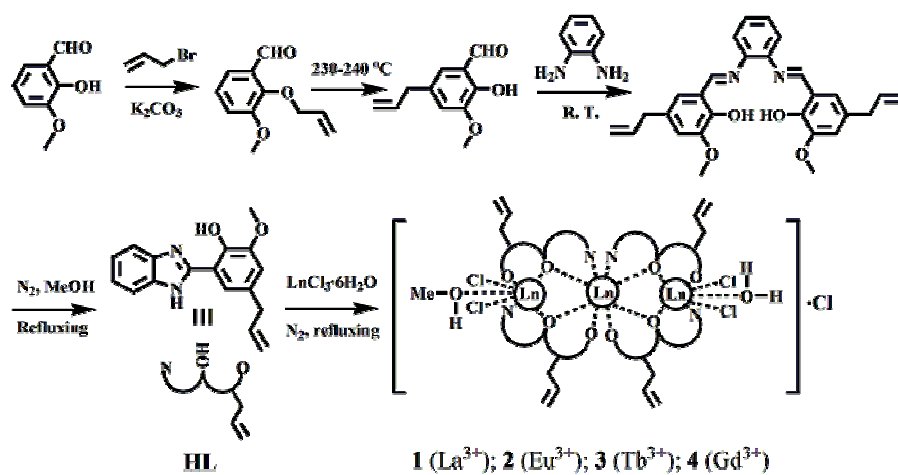
400:1 in solid state.

**Figure 10** Visible emission and excitation spectra of **PMMA@2** and **PMMA@4**, or **Poly(NBE-2)** and **Poly(NBE-4)** with the feeding molar ratio of 400:1 in solid state at RT.

**Figure 11** Emission and excitation spectra of the hybrid materials **3@PMMA** (11a) or **Poly(NBE-3)** (11b) from different feeding molar ratios (200:1, 400:1, 600:1 and 800:1) in solid state at RT.

**Figure 12** CIE chromaticity graphs with the same color coordinate ( $x = 0.30$ ,  $y = 0.60$ ) for the emissions of **3@PMMA** and **Poly(NBE-3)** with the feeding molar ratio of 400:1 in solid state.

Scheme 1



Scheme 2

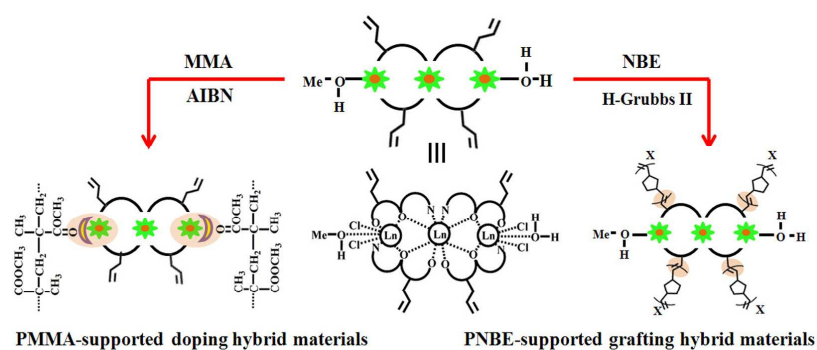


Figure 1

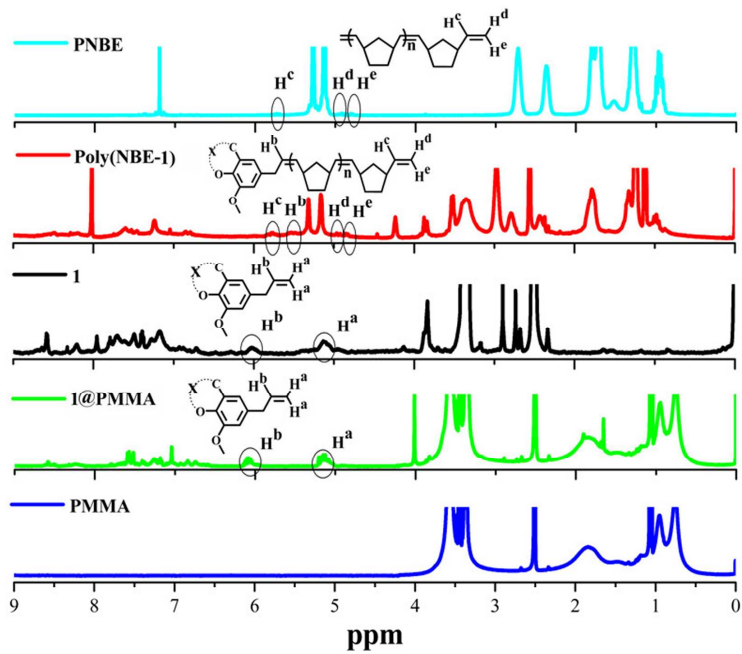
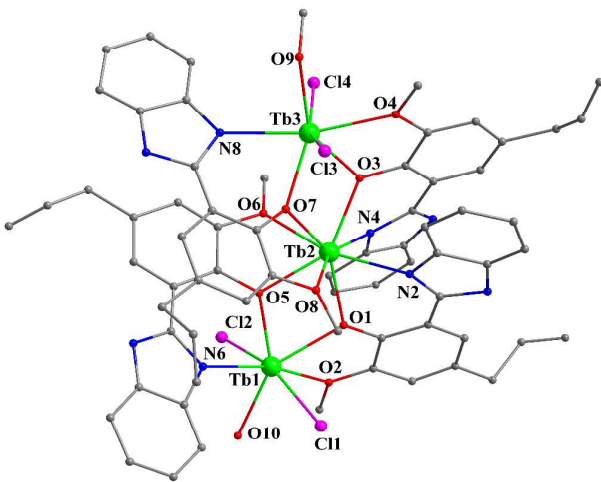
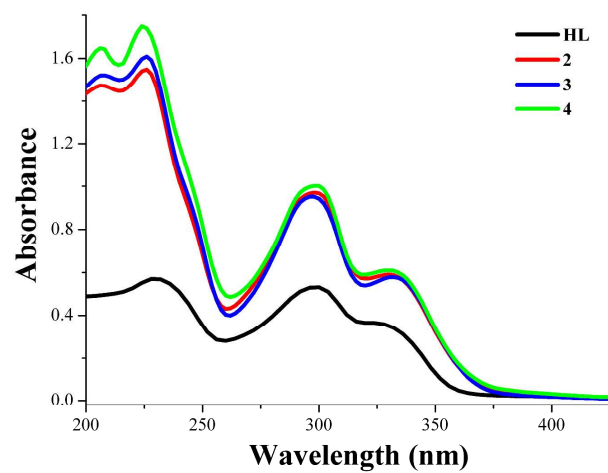


Figure 2





### Figure 3



**Figure 4**

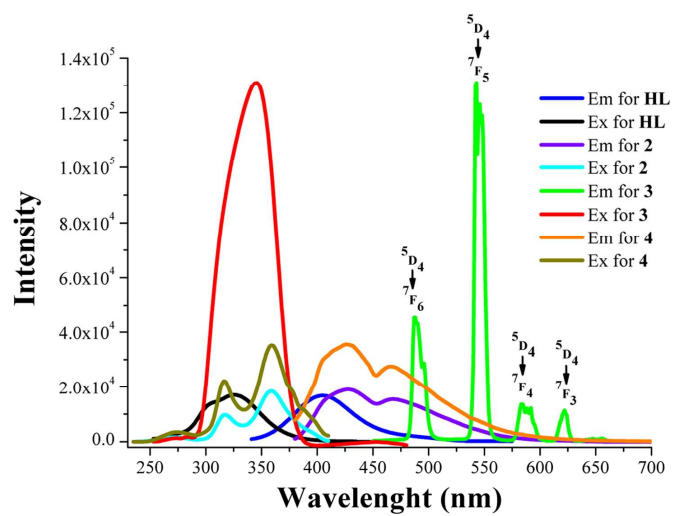


Figure 5

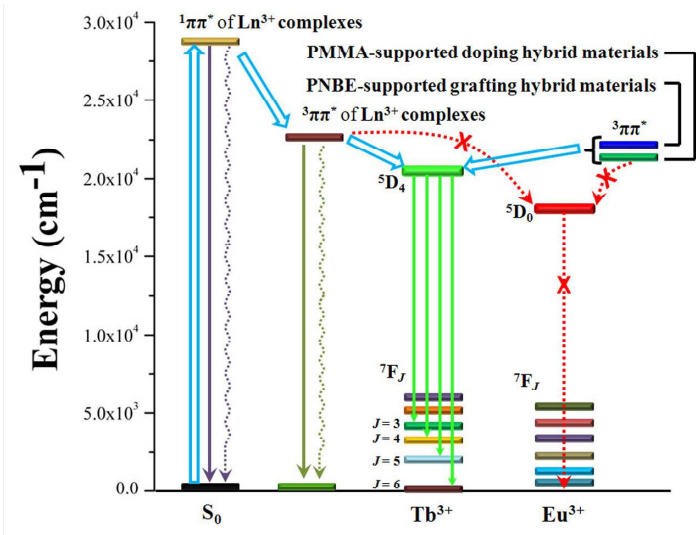


Figure 6

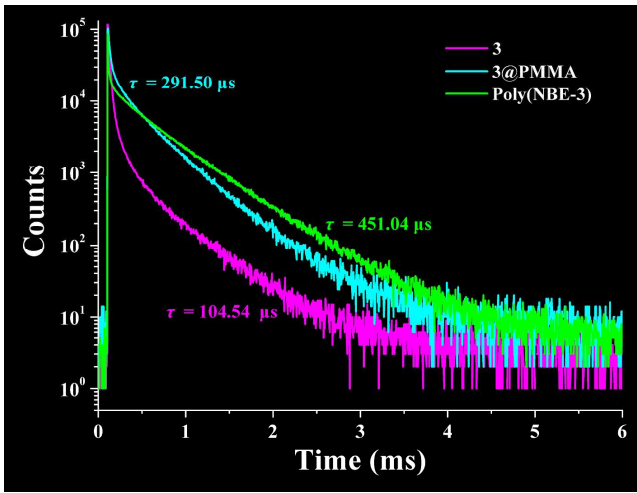


Figure 7

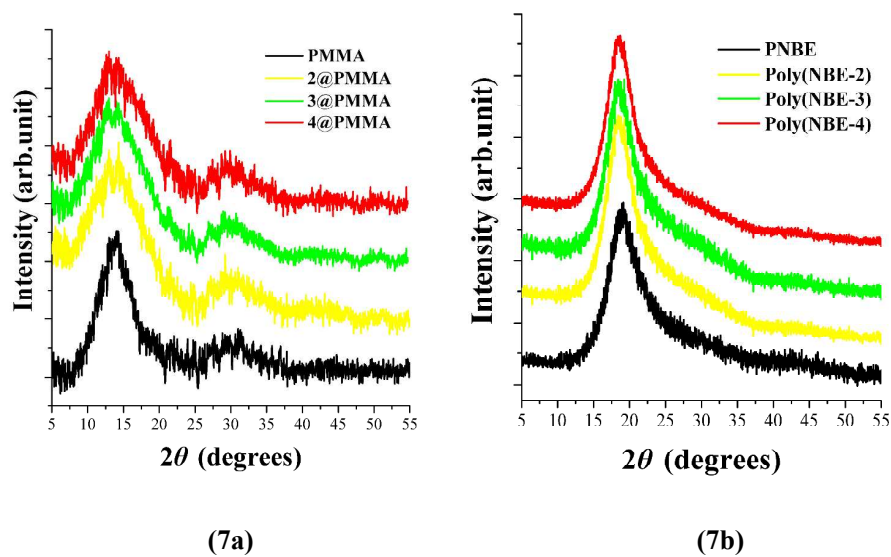


Figure 8

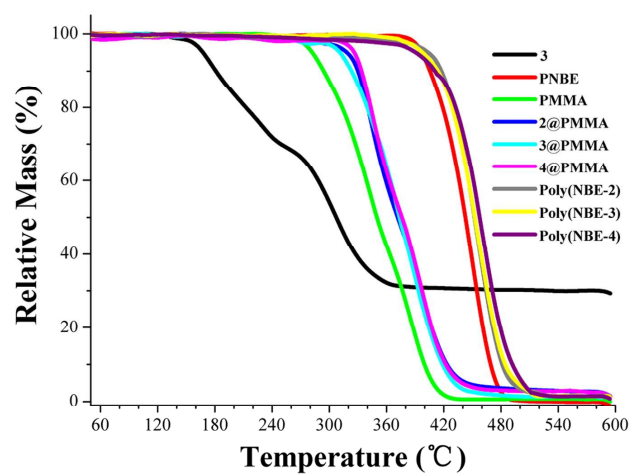


Figure 9

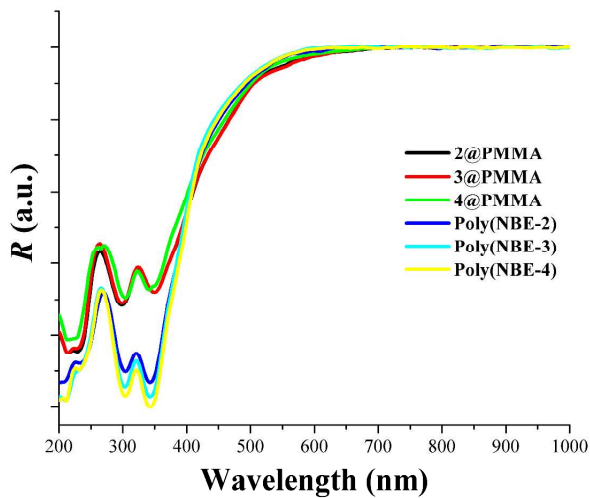


Figure 10

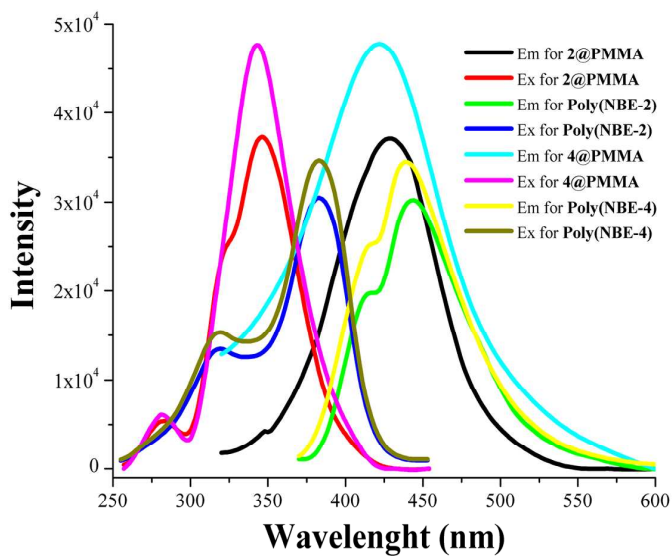


Figure 11

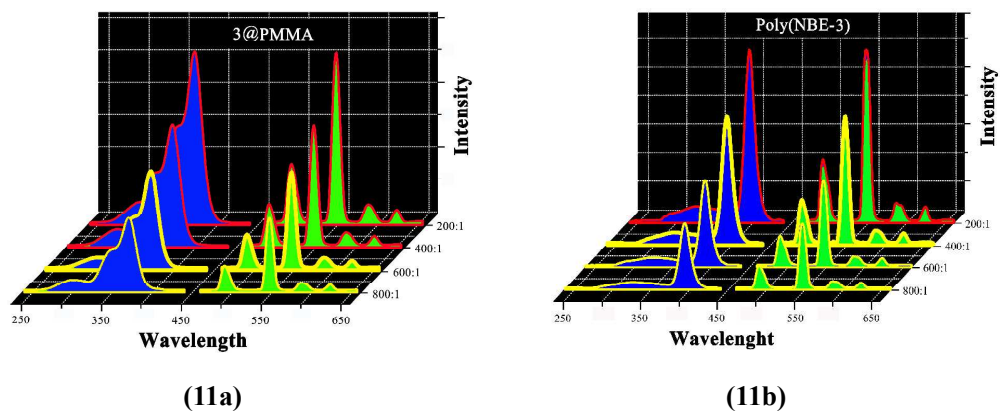


Figure 12

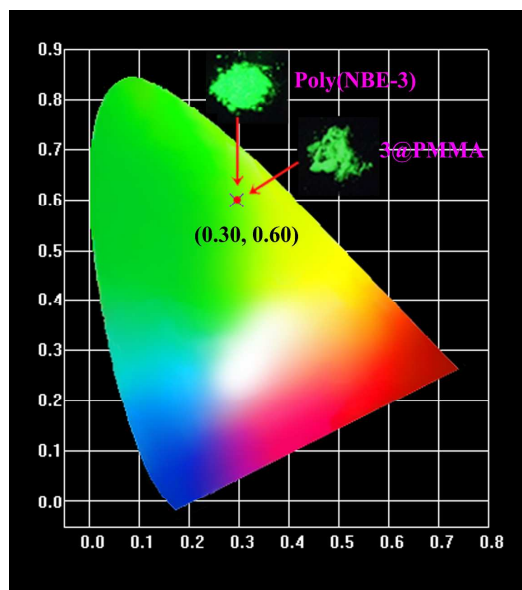


Table of content

In the obtained Tb<sup>3+</sup>-based efficient ( $\Phi_{\text{overall}} = 76\text{-}83\%$ ) and high color-purity green luminescent **3@PMMA** from doping and metallopolymer-type **Poly(NBE-3)**, the grafting endows the higher-concentration self-quenching as compared to the physical doping.

